Accepted to AJ
Preprint typeset using LaTeX style emulateapj v. 6/22/04

MMT EXTREMELY METAL POOR GALAXY SURVEY I. AN EFFICIENT TECHNIQUE TO IDENTIFY METAL POOR GALAXIES

Warren R. Brown
Smithsonian Astrophysical Observatory

Lisa J. Kewley[1]
University of Hawaii

and

Margaret J. Geller
Smithsonian Astrophysical Observatory
Accepted to AJ

ABSTRACT

We demonstrate a successful strategy for identifying extremely metal poor galaxies. Our preliminary survey of 24 candidates contains 10 metal poor galaxies of which 4 have $\log(\mathrm{O/H}) + 12 < 7.65$, some of the lowest metallicity blue compact galaxies known to date. Interestingly, our sample of metal poor galaxies have systematically lower metallicity for their luminosity than comparable samples of blue compact galaxies, dIrrs, and normal star-forming galaxies. Our metal poor galaxies share very similar properties, however, with the host galaxies of nearby long-duration gamma-ray bursts (GRBs), including similar metallicity, stellar ages, and star formation rates. We use Hβ to measure the number of OB stars present in our galaxies and estimate a core-collapse supernova rate of $\sim 10^{-3}$ yr^{-1}. A larger sample of metal poor galaxies may provide new clues into the environment where GRBs form and may provide a list of potential GRB hosts.

Subject headings: galaxies: abundances — galaxies: starburst — gamma rays: bursts

1. INTRODUCTION

Metal poor galaxies are the key to understanding star formation and gas enrichment in a nearly pristine interstellar medium, and may provide a template for understanding the formation of the first stars. Extremely metal poor galaxies (XMPGs) are extremely rare: fewer than 1% of dwarf galaxies are XMPGs, with a gas-phase oxygen abundance $\log(\mathrm{O/H}) + 12 \leq 7.65$ (Kunth & Östlin 2000; Kniazev et al. 2003). Known XMPGs are mostly gas-rich, blue compact galaxies with spectra dominated by emission lines. The first surveys to search for XMPGs were objective prism surveys (MacAlpine et al. 1977; Kunth et al. 1981; Terlevich et al. 1991). Abundance studies of these surveys revealed up to a dozen XMPGs (Kunth & Sargent 1983; Campbell et al. 1986; Masegosa et al. 1994), but none so extreme as I Zw 18 (Searle & Sargent 1972). I Zw 18, now along with SBS 0335-052W and DDO 68, are the most metal poor local galaxies known, with $\log(\mathrm{O/H}) + 12$ ranging 7.12 - 7.17 (Izotov et al. 2005; Izotov & Thuan 2007). Papaderos et al. (2006) found 2 new XMPGs in the 2dF survey. Among the 1,000,000 spectra released by the Sloan Digital Sky Survey (SDSS), there are 19 identified XMPGs (Kniazev et al. 2003; Izotov et al. 2004, 2006a; Izotov & Thuan 2007), emphasizing the rarity of such objects.

Kewley et al. (2007) recently announced the serendipitous discovery of a new XMPG, SDSS J080840.85+172856.48 (hereafter SDSS J0809+1729). The object is a stellar point source in the SDSS catalog. It was observed as part of the Brown et al. (2006a) hypervelocity star survey on the basis of its stellar B-type photometric colors. Spectroscopy reveals that the object is not a star but rather a compact blue galaxy at $cz = 13232$ km s^{-1}. Our re-analysis shows that the galaxy has $\log(\mathrm{O/H}) + 12 = 7.48 \pm 0.1$. Interestingly, the observed electron density, star formation rate, and total luminosity of this XMPG are remarkably similar to nearby GRB host galaxies (Kewley et al. 2007).

Nearby $z < 0.2$ long duration GRBs are observed in metal poor galaxies (Prochaska et al. 2004; Sollerman et al. 2005; Fruchter et al. 2006; Stanek et al. 2006; Wolf & Podsiadlowski 2007; Wiersema et al. 2007; Margutti et al. 2007). Fruchter et al. (2006) argue that the link between metal poor galaxies and GRBs originates in the atmospheres of massive stars. Massive metal poor stars lack the opacity to support significant stellar winds, and thus can produce the anomalous Type 1c supernovae associated with nearby GRBs. Berger et al. (2007) argue that GRBs are linked to young starburst populations, which at low redshift happen to be found predominantly in low mass, metal-poor galaxies. At large redshift $z > 0.2$, the metallicity of GRB hosts is much harder to determine (Prochaska 2006). At least one GRB host galaxy is an extremely red and probably metal rich object (Berger et al. 2007), and other GRB hosts $0.2 < z < 1$ appear consistent with normal metallicity-luminosity relations (Wolf & Podsiadlowski 2007; Margutti et al. 2007). GRBs clearly occur in different types of host galaxies; they are not tied exclusively to the most metal poor galaxies. Yet finding and studying metal poor galaxies with properties similar to nearby GRB host galaxies may yield critical clues about the environment where nearby GRBs form.

Electronic address: wbrown@cfa.harvard.edu
[1] Hubble Fellow

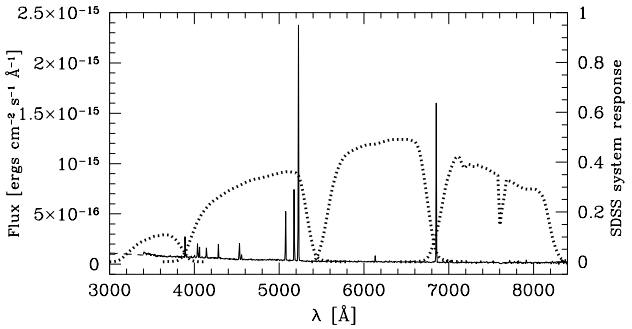

FIG. 1.— Observed spectrum of the XMPG SDSS J0809+1729 (Kewley et al. 2007) plotted against the total system throughput of the SDSS u' g' r' i' filter bandpasses (dotted lines). The strong emission line contribution to the galaxy's broadband magnitudes results in unusual colors that vary with redshift.

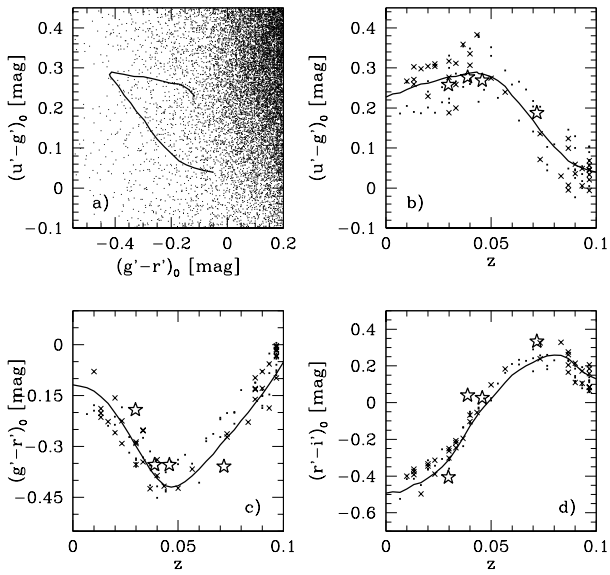

FIG. 2.— Target selection for our MMT survey for XMPGs. a) Color-color plot showing all SDSS DR4 galaxies (dots) and the color-redshift track for the XMPG J0809+1729 (solid line). b) - d) Color-redshift plots showing SDSS objects (dots) that simultaneously match all three color-redshift tracks (solid lines) within 0.1 mag. After removing saturated stars and nearby HII regions by visual inspection, we are left with a sample of 38 XMPG candidates (x's). Four new XMPGs discovered by this survey are indicated by stars.

Inspired by the discovery of SDSS J0809+1729, we designed a survey to find metal poor galaxies. We use a technique similar to photometric redshifts to identify metal poor galaxies in the SDSS galaxy catalog. We test this technique and target $g' \sim 20$ galaxies with very blue colors, a region of parameter space not well probed by previous surveys. Our strategy uncovers 10 metal poor galaxies from a sample of 24 candidates, 4 of which are new XMPGs.

In §2 we present our technique to find new metal poor galaxies and discuss the efficacy of our survey. In §3 we describe the properties of the entire set of metal poor galaxies, and compare the galaxies with samples of blue compact galaxies and nearby GRB hosts. In §4 we estimate the expected core-collapse supernova rate in our galaxies. We conclude in §5.

2. DATA

2.1. *Technique to Find Extremely Metal Poor Galaxies*

Known XMPGs outside the Local Group are starburst galaxies characterized by very low internal extinction, high ionization parameter, and large gas-phase electron density (e.g. Kniazev et al. 2003; Izotov et al. 2005, 2006a; Papaderos et al. 2006; Kewley et al. 2007; Izotov & Thuan 2007). As a result, XMPGs have steep blue continua, large [OIII]/[OII] ratios, and strong hydrogen Balmer emission lines. These characteristics significantly affect the broadband colors of XMPGs. For example, Figure 1 shows the observed spectrum of SDSS J0809+1729 plotted against the total system throughput of the SDSS $u'g'r'i'$ filter bandpasses[2]. The contribution of emission lines to the broadband magnitudes of SDSS J0809+1729 is approximately 3%, 32%, 6%, and 12% at u', g', r', and i' respectively.

The strong emission line contribution to XMPGs' broadband magnitudes results in unusual colors that change with redshift. For example, at lower redshift, SDSS J0809+1729 does not satisfy the B-star criteria in Brown et al. (2006b) because Hα drops into the r' band and produces a much redder $(g' - r')$ color. Conversely, at higher redshift, Hβ and O III move from g' into r' and also produce a much redder $(g' - r')$ color (see Figure 1). We quantify these effects using the RVSAO package (Kurtz & Mink 1998) to shift the XMPG spectra to different redshifts. We predict the galaxy's colors at different redshifts by adding the *relative* change in color to the observed photometry. In effect, we are calculating k-corrections for the XMPG.

Figure 2 plots the resulting color-redshift tracks for SDSS J0809+1729 (solid lines). Over the range $0.0 < z < 0.10$, the XMPG's $(u' - g')_0$ and $(g' - r')_0$ colors vary by $\sim$ 0.3 mag and the $(r' - i')_0$ color varies by $\sim$1 mag. The subscript 0 indicates colors corrected for Galactic extinction following Schlegel et al. (1998). We note that the Johnson/Cousins passbands are much less sensitive than their SDSS equivalents because the strong Hβ/[O III] and Hα emission lines remain in their respective V and R passbands for $0.0 < z < 0.10$.

Knowing how the broadband colors of an XMPG change with redshift, we can search for new XMPGs at other redshifts in the SDSS photometric catalog. Unfortunately, searching for new XMPGs like SDSS J0809+1729 in the stellar catalog is not feasible because of immense contamination from white dwarfs with similar colors. Instead, we search the SDSS galaxy catalog.

We use the color-redshift track of our newly discovered XMPG, SDSS J0809+1729, as the basis for the sample of XMPGs published here. We begin by selecting all galaxies in SDSS DR4 (Adelman-McCarthy et al. 2006) with $g' < 20.5$. Figure 2a plots these galaxies with similar $(u' - g')_0$ and $(g' - r')_0$ to SDSS J0809+1729. Only by combining two or more colors can we meaningfully select XMPG candidates. We find $\sim 10^3$ galaxies simultaneously within 0.1 mag of any pair of color-redshift tracks, and a mere 107 galaxies (small squares, Figure 2b-d) si-

[2] http://www.sdss.org/dr5/instruments/imager/index.html

multaneously within 0.1 mag of all three color-redshift tracks. We visually inspect the objects and find that many are near saturated stars or that they are HII regions in nearby galaxies. After eliminating the unwanted objects, we are left with a sample of 38 photometrically-selected XMPG candidates (marked by x's, Figure 2b-d). Our survey is based on this sample of 38 XMPG candidates.

We use a restrictive color selection as the first demonstration of our technique. If our XMPG selection strategy is successful, we can easily broaden the search parameters to identify many more faint XMPG candidates.

2.2. *Observations*

We obtained spectroscopy of the 24 candidates available on the nights of 2006 May 25-27 and 2006 June 19-20. Table 1 lists the 24 candidates. Observations were obtained with the 6.5m MMT telescope and the Blue Channel spectrograph. We operated the spectrograph with the 300 line mm^{-1} grating and a 1″ slit. These settings provide a wavelength coverage of 3400 Å to 8600 Å and a spectral resolution of 6.2 Å. Exposure times were typically 30 minutes. We obtained comparison lamp exposures after every exposure.

We reduce the spectra using standard IRAF[3] spectral reduction tasks and measure recession velocities from emission lines using the package RVSAO (Kurtz & Mink 1998). We flux calibrate using spectrophotometric standards (Massey et al. 1988) and the standard Kitt Peak atmospheric extinction correction. For objects obtained in non-photometric conditions, we scale the spectra by the flux ratio of the observed spectroscopic and SDSS broadband magnitudes. We estimate that absolute flux calibration is accurate to ∼25%.

We measure emission line fluxes using IRAF *splot* and *fitprof* tasks, and find no significant offset between the two methods. Table 2 presents the observed line strengths with their measurement uncertainties. The statistical uncertainties are formally a few percent, but the true error is dominated by uncertainties in the reddening correction, the stellar absorption correction, and the absolute flux calibration.

For our analysis, we correct the observed emission line fluxes for reddening using the Balmer decrement and the Cardelli et al. (1989) reddening curve. We assumed an $R_V = A_V/\mathrm{E}(B-V) = 3.1$ and an intrinsic $\mathrm{H}\alpha/\mathrm{H}\beta$ ratio of 2.85 (the Balmer decrement for case B recombination at T= 10^4K and $n_e \sim 10^2 - 10^4 \mathrm{cm}^{-3}$; Osterbrock 1989).

We find no evidence for stellar absorption in the expected sense. While one would expect some underlying stellar absorption, we do not see Stark-broadened absorption in the wings of the Balmer emission lines. The de-reddened Balmer emission line ratios exhibit a 7% scatter around the Osterbrock (1989) values for case B recombination at T= 10^4 K. If we apply a constant 2 Å equivalent width correction, appropriate for the young 4-5 Myr stellar age of the galaxies (see §3.4), the scatter of the Balmer line ratios around the Osterbrock (1989) values remains unchanged at 7%. We conclude that stellar absorption is smaller than the uncertainty in the line ratio measurements.

[3] IRAF is distributed by the National Optical Astronomy Observatories, which are operated by the Association of Universities for Research in Astronomy, Inc., under cooperative agreement with the National Science Foundation.

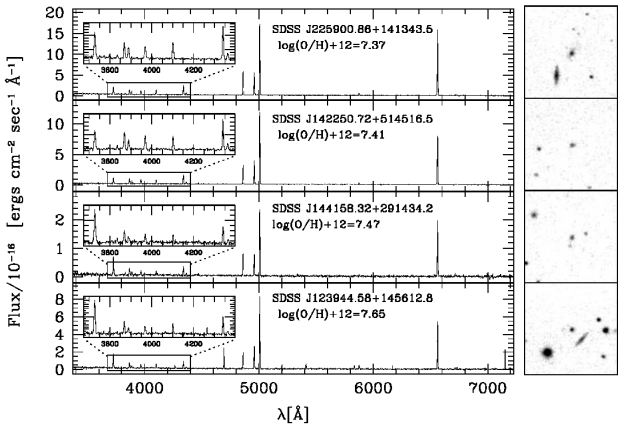

FIG. 3.— MMT spectra of our 4 new XMPGs. [O III] λ4363 is well-detected in all four objects (see insets). The extremely weak [NII] and [SII] lines visibly indicate the extremely low abundance of these objects. The thumbnail images, courtesy of SDSS, are 48″on a side and show that all 4 XMPGs appear to be compact dwarfs.

We calculate electron densities with the S II λ6717 / S II λ6731 line ratio, when present, in conjunction with a 5 level model atom using the Mappings photoionization code (Sutherland & Dopita 1993). We derive the gas-phase oxygen abundance following the procedure outlined in Izotov et al. (2006b) within the framework of the classical two-zone HII-region model (Stasinska 1980). This procedure utilizes the electron-temperature T_e calibrations of Aller (1984) and the atomic data compiled by Stasińska (2005).

The gas-phase oxygen abundance depends on line ratios and thus is independent of the uncertainties in our absolute flux calibration. We propagate the errors from the line ratio measurement, the extinction correction, and the stellar absorption correction, and find that the relative errors in metallicities derived using the same method are formally ≤ 0.07 dex. However, the absolute error is at least ∼ 0.1 dex. Thus systematics dominate the errors; our metallicities are accurate at the ±0.1 dex level.

2.3. *Survey Efficiency*

Our initial survey of 24 candidates contains 10 metal poor galaxies with log(O/H) + 12< 8 of which 4 are new XMPGs. Thus our strategy is ∼20% efficient for selecting XMPGs. Spectra and thumbnail images of the 4 new XMPGs are displayed in Figure 3 (see also Table 3). Three of the new XMPGs (SDSS J142250.72+514516.5, SDSS J144158.32+291434.2 and SDSS J225900.86+141343.5) have lower abundance than SDSS J0809+1729. The remaining objects in our survey are either A stars in the Milky Way, galaxies with modest emission lines, and a few odd objects (one E+A, one possible BL Lac, one possible quasar) listed in Table 1.

3. GALAXY PROPERTIES

We now open our discussion to include all the metal poor galaxies in our survey. Including SDSS J0809+1729, our survey contains 5 XMPGs and 6 metal poor galaxies. Table 3 summarizes the spectroscopic

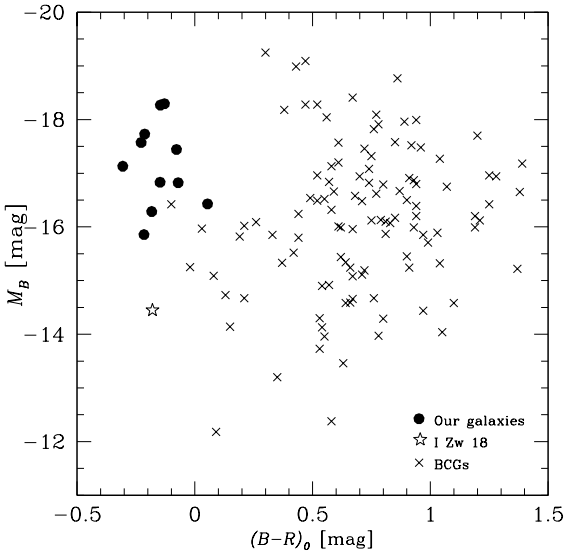

FIG. 4.— Color-magnitude distribution of nearby BCGs (Gil de Paz et al. 2003) and our 11 metal poor galaxies, for which we estimate $(B-R)$ from SDSS photometry (Fukugita et al. 1996).

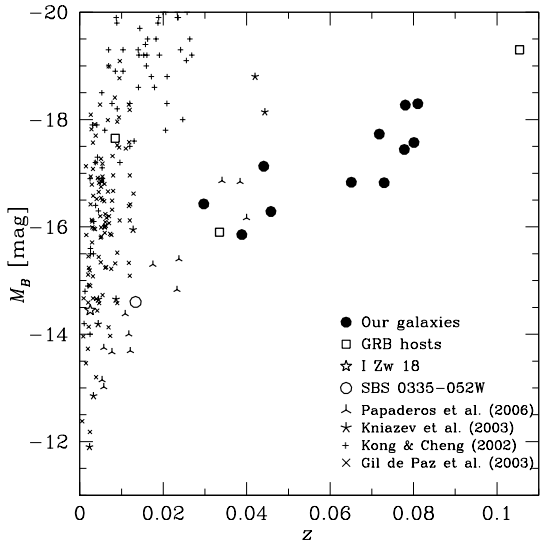

FIG. 5.— Redshift and luminosity distribution of BCGs (Kong & Cheng 2002; Gil de Paz et al. 2003), metal poor galaxies from 2dF (Papaderos et al. 2006) and SDSS (Kniazev et al. 2003), our 11 metal poor galaxies, and the 3 nearest GRB host galaxies (Stanek et al. 2006). M_B is calculated for the 2dF galaxies assuming $(B-V)=0.5$ (Papaderos et al. 2006). M_B is estimated for the SDSS galaxies from SDSS photometry (Kniazev et al. 2003).

measurements for the 11 galaxies. Because the galaxies are compact objects, our spectra provide reasonable global estimates of their properties. We compare the properties of our galaxies with similar samples of blue compact galaxies (BCGs) and with nearby GRB hosts. Throughout this paper we adopt a flat, Λ-dominated cosmology with $H_o = 70$ and $\Omega_m = 0.3$.

3.1. *Color and Redshift Distribution*

Our 11 metal poor galaxies are systematically bluer and more luminous than other known BCGs. Figure 4 plots the Gil de Paz et al. (2003) sample of nearby BCGs, for which $(B-R)_0$ and M_B are all available. We estimate $(B-R)$ for our galaxies from SDSS photometry (Fukugita et al. 1996), and shift the observed magnitudes to the rest-frame using k-corrections we calculate for B and R passbands as described in §2. It is clear that our metal poor galaxies are more than 0.5 mag bluer in $(B-R)_0$ than most nearby BCGs. I Zw 18 and UCM 1612+1308 (Rego et al. 1998) are the two BCGs with colors comparable to our metal poor galaxies. However, our metal poor galaxies are systematically more luminous than the BCGs with similar colors.

Our 11 metal poor galaxies are also at greater redshift than most known BCGs. Figure 5 plots the redshift distribution of BCGs (Kong & Cheng 2002; Gil de Paz et al. 2003), metal poor galaxies from 2dF (Papaderos et al. 2006) and SDSS (Kniazev et al. 2003), our 11 metal poor galaxies, and the 3 nearest GRB host galaxies (Stanek et al. 2006). Note that we calculate M_B for the 2dF galaxies assuming the average $(B-V)=0.5$ for that sample (Papaderos et al. 2006). We estimate M_B for the SDSS galaxies from g' and r' photometry in Kniazev et al. (2003). Figure 5 shows that the vast majority of known BCGs have redshifts $z < 0.02$. The 2dF and SDSS surveys access fainter magnitudes than earlier BCG samples and thus contain a number of very low luminosity galaxies, plus a few higher luminosity metal poor galaxies at $z \sim 0.04$. Our sample of metal poor galaxies, by construction, spans the range $0.02 < z < 0.08$. Searching a large volume of space enables the discovery of rare objects like XMPGs.

3.2. *Luminosity-Metallicity Relation*

Luminosity-metallicity relations are well determined for galaxies ranging from large star-forming galaxies (e.g. Tremonti et al. 2004) to dwarf irregulars (e.g. Richer & McCall 1995). The physical basis for the luminosity-metallicity relation is a mass-metallicity relation: low mass galaxies are thought to sustain less star formation and retain fewer metals than high mass galaxies. We now compare the luminosity and metallicity of our galaxies with samples of comparable metal-poor dwarf galaxies. Because there is some disagreement about the calibration of different metallicity-estimate methods, we only consider galaxy samples with metallicities derived with the T_e method.

Figure 6 plots samples of BCGs (Kong & Cheng 2002; Shi et al. 2005), metal poor galaxies from 2dF (Papaderos et al. 2006) and SDSS (Kniazev et al. 2003), our metal poor galaxies, and four nearby GRB host galaxies (Stanek et al. 2006). We use metallicities for the GRB hosts calculated using the T_e method as described in Kewley et al. (2007). Figure 6 shows that our sample of galaxies has either 1) lower metallicity by ∼0.5 dex than the Richer & McCall (1995) luminosity-metallicity relation for normal dIrrs, or 2) higher luminosity by 3 - 5 mag in M_B.

Other samples of nearby, metal poor galaxies exhibit a large scatter around the luminosity-metallicity relation (Kunth & Östlin 2000). Yet our galaxies appear unusual because of their large *systematic* offset from the luminosity-metallicity relation. We will use population

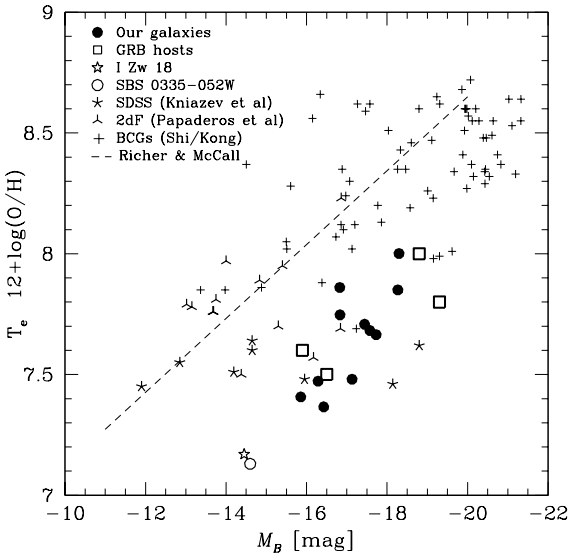

FIG. 6.— Luminosity-metallicity plot for BCGs (Kong & Cheng 2002; Shi et al. 2005), metal poor galaxies from 2dF (Papaderos et al. 2006) and SDSS (Kniazev et al. 2003), our metal poor galaxies, and four nearby GRB host galaxies (Stanek et al. 2006). Our sample of metal poor galaxies fills in the region defined by the GRB hosts; all these galaxies have lower metallicity by ∼0.5 dex than the Richer & McCall (1995) luminosity-metallicity relation (*dashed line*) for normal dIrrs.

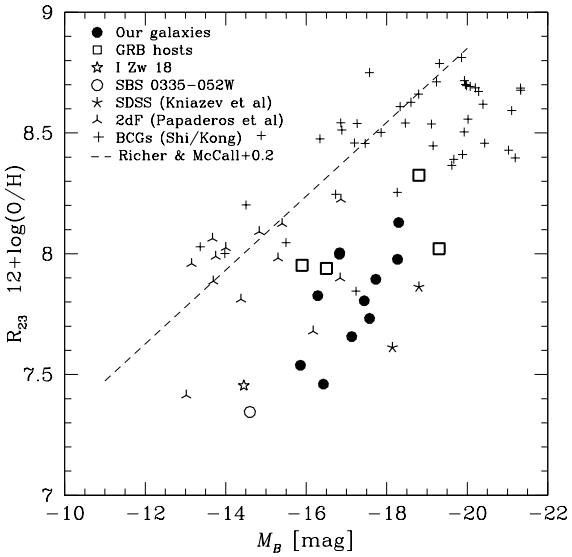

FIG. 7.— Same as Figure 6, except we plot strong line metallicities calculated using R_{23} McGaugh (1991). The strong line metallicities are systematically +0.2 dex larger than the T_e metallicities, but the overall distribution remains the same: our sample of metal poor galaxies and the GRB hosts are systematically offset from the Richer & McCall (1995) luminosity-metallicity relation (*dashed line*), which we shift by +0.2 dex for consistency.

synthesis models to address the evolutionary paths of our metal poor galaxies in a future paper.

Remarkably, our sample of metal poor galaxies fills the region of the luminosity-metallicity diagram outlined by nearby GRB host galaxies. The only other galaxies with similar properties are the five metal poor 2dF and SDSS galaxies at $z \sim 0.04$: 2dF 169299, 2dF 115901, SDSSJ051902.64+000730.0, SDSSJ104457.84+035313.2, and SDSSJ084030.00+470710.2. The nearby BCG II Zw 70 also appears to fall in the region defined by the GRB hosts.

The relative distribution of galaxies in the luminosity-metallicity plot does not change with different metallicity estimators. To illustrate this point, we calculate strong line metallicities using R_{23} (McGaugh 1991) for the entire set of galaxies. The results are plotted in Figure 7. The R_{23} metallicities have an average offset of +0.2 dex from the T_e metallicities, and so we shift the Richer & McCall (1995) luminosity-metallicity relation in Figure 7 by a constant +0.2 dex for consistency. Yet the relative distribution of galaxies remains the same: our metal poor galaxies (and the GRB host galaxies) maintain a large, systematic offset from the luminosity-metallicity relation defined by normal dIrrs and BCGs.

3.3. *Extinction*

Our sample of 11 metal poor galaxies suffer from very little internal extinction. Table 3 lists the Balmer Hα/Hβ ratios, which average 2.8±0.2. The intrinsic Hα/Hβ ratio is 2.86 for case B recombination at T= 10^4 K and $n_e \sim 10^2 - 10^4$ cm^{-3} (Osterbrock 1989). Low extinction is expected in low metallicity galaxies, and is also observed in nearby GRB hosts (e.g. Kewley et al. 2007).

3.4. *Star Formation Age and Rates*

XMPGs remain a puzzle because they may be pristine galaxies undergoing their first burst of star formation or they may contain older stellar population from previous episodes of star formation. *Hubble Space Telescope* images resolve old stellar populations in the nearest metal poor galaxies. I Zw 18, for example, has stars with ages ranging from ∼ 500 Myr (Izotov & Thuan 2004) to ∼ 1 Gyr (Aloisi et al. 1999). Although we cannot estimate the age of old stellar populations (if any) in our metal poor galaxies, stellar population synthesis models provide an estimate of the age of the young stellar population.

We estimate the stellar age of our metal poor galaxies from the Hβ equivalent width following Schaerer & Vacca (1998). Under the assumption of a Salpeter initial mass function and an instantaneous burst of star formation, the stellar ages of our metal poor galaxies are in the range 4 - 5 Myr (see Table 3).

Star formation rates (SFRs) are more difficult to estimate because traditional calibrations are not applicable to extremely metal poor objects. We use the calibration derived by Kewley et al. (2007) based on the stellar population synthesis models of Bicker & Fritze-v. Alvensleben (2005). Our metal poor galaxies then have SFRs in the range 0.1 - 0.5 $M_\odot$ yr^{-1} (Table 3). Both the stellar ages and SFRs of our metal poor galaxies are remarkably similar to those found for nearby GRB hosts (Kewley et al. 2007).

4. SUPERNOVA RATES AND THE GRB CONNECTION

We next ask how frequently GRBs might occur in our sample of metal poor galaxies, if GRBs are indeed associated with core-collapse supernova in metal poor galaxies. We start by estimating the number of massive O and B

stars in our sample of 11 galaxies, and then estimate the rate of core-collapse supernovae.

Under the assumption of an ionization-bounded nebula, the Hβ line luminosity provides an estimate of the ionizing flux present in the galaxies. The metal poor galaxies suffer from very little extinction, as measured by their Hα/Hβ ratios; thus we make no correction for internal extinction. We follow Schaerer & Vacca (1998) and convert the observed Hβ ionizing flux to an equivalent number of O stars. We select the "equivalent O7V to O star" ratio η_o based on the stellar age and metallicity of the galaxy; η_o values range from 0.25 - 0.5. The minimum O star mass is $\sim$13.3 $M_\odot$ at our metallicities (Vacca 1994). However, core-collapse supernovae will result from B stars with masses as low as $\sim$8 $M_\odot$. A Salpeter initial mass function has the same number of O stars with 13 - 120 $M_\odot$ as B stars with 8 - 13 $M_\odot$. Thus, the total number of core-collapse supernova progenitors is roughly twice the Schaerer & Vacca (1998) number of equivalent O stars. We list our estimate of the total number of core-collapse supernova progenitors in the column n(OB) (Table 3). On average, there are $\sim$25,000 potential core-collapse supernova progenitors per galaxy in our sample. This number may appear relatively small, but the metal poor galaxies are dwarfs, not massive galaxies.

We estimate core-collapse supernova rates in our metal poor galaxies by assuming supernovae occur uniformly over the lifetime of the longest-lived progenitor. The Schaller et al. (1992) stellar evolution track for a 9 $M_\odot$ star with $Z = 0.001$ has a lifetime of 30 Myr. Thus the average rate of core-collapse supernovae in our metal poor galaxies is $\sim 10^{-3}$ yr^{-1}, with an uncertainty of a factor of a few. In other words, a couple thousand such metal poor galaxies must be monitored to witness one core-collapse supernova per year. A typical spiral galaxy, in comparison, has a typical SFR of $\sim$10 $M_\odot$ yr^{-1} (e.g. Brinchmann et al. 2004) and a core-collapse supernova rate $\sim$100 times larger than the metal poor galaxies, assuming a constant SFR and Salpeter initial mass function.

The ratio of GRBs to core-collapse supernovae events depends on how narrowly beamed GRBs are. If 1 out of 100 core-collapse supernovae appear as GRBs, then a sample of a $\sim 10^5$ metal poor galaxies must be monitored to witness one GRB per year. There is currently little constraint on the space density of metal poor galaxies, in part because they are such low-luminosity systems. Surveys reaching faint magnitude limits may uncover large numbers of new metal poor galaxies. However, it may be difficult to detect a supernova coincident on the high surface-brightness core of these galaxies. Figure 3 shows that the four XMPGs, for example, are compact systems. Although metal poor galaxies are potential GRB hosts, a survey to find GRBs by monitoring a sample metal poor galaxies appears impractical currently. Future deep imaging surveys, such as Pan-STARRS and the Large Synoptic Survey Telescope (LSST), may be able to detect supernovae in these low-luminosity galaxies.

5. CONCLUSIONS

We have designed a successful strategy to find new metal poor galaxies. We calculate the expected colors of metal poor galaxies at different redshifts based on the spectrum of the newly discovered XMPG, SDSS J0809+1729 (Kewley et al. 2007). We observed an initial sample of 24 candidates with the MMT telescope and find 4 new XMPGs with log(O/H) + 12$\leq$ 7.65, a $\sim$20% selection efficiency.

Our full set of 11 metal poor galaxies are systematically bluer and more luminous than comparable samples of BCGs. Our galaxies are also systematically more metal poor by 0.5 dex (or more luminous by 3 - 5 mag) than samples of BCGs, dIrrs, and other metal-poor dwarf galaxies. Remarkably, our galaxies share the same region of the luminosity-metallicity diagram with nearby GRB hosts. The similarity in extinction, stellar age, and star formation rates suggests that our metal poor galaxies are potential hosts for GRBs.

We estimate an average core-collapse supernova rate $\sim 10^{-3}$ yr^{-1} in our metal poor galaxies. This estimate comes from an estimate of the number of O and B stars in the galaxies. If GRBs are indeed linked to core-collapse supernova in metal poor galaxies, future surveys such as Pan-STARRS or LSST may be able to find GRBs by monitoring a large sample of metal poor galaxies.

The success of our XMPG selection strategy allows us to expand our survey. For example, using the new XMPGs (Figure 3) as additional templates, we identify a total of 335 XMPG candidates in SDSS Data Release 5. Spectroscopic observations of these XMPG candidates are underway.

W. R. Brown was supported in part by a Clay Fellowship during this work. L. J. Kewley was supported by a Hubble Fellowship. We thank S. Kenyon and the anonymous referee for comments that greatly improved this paper. This research has made use of NASA's Astrophysics Data System Bibliographic Services. This project makes use of data products from the Sloan Digital Sky Survey, which is managed by the Astrophysical Research Consortium for the Participating Institutions. We thank the Smithsonian Institution for partial support of this research.

Facilities: MMT (Blue Channel Spectrograph)

REFERENCES

Adelman-McCarthy, J. K. et al. 2006, ApJS, 162, 38
Aller, L. H. 1984, in Astrophysics & Space Science Library vol. 112, ed. L. H. Aller
Aloisi, A., Tosi, M., & Greggio, L. 1999, AJ, 118, 302
Berger, E., Fox, D. B., Kulkarni, S. R., Frail, D. A., & Djorgovski, S. G. 2007, ApJ, 660, 504
Bicker, J. & Fritze-v. Alvensleben, U. 2005, A&A, 443, L19
Brinchmann, J., Charlot, S., White, S. D. M., Tremonti, C., Kauffmann, G., Heckman, T., & Brinkmann, J. 2004, MNRAS, 351, 1151
Brown, W. R., Geller, M. J., Kenyon, S. J., & Kurtz, M. J. 2006a, ApJ, 640, L35
—. 2006b, ApJ, 647, 303 (Paper I)
Campbell, A., Terlevich, R., & Melnick, J. 1986, MNRAS, 223, 811
Cardelli, J. A., Clayton, G. C., & Mathis, J. S. 1989, ApJ, 345, 245
Fruchter, A. S. et al. 2006, Nature, 441, 463
Fukugita, M., Ichikawa, T., Gunn, J. E., Doi, M., Shimasaku, K., & Schneider, D. P. 1996, AJ, 111, 1748
Gil de Paz, A., Madore, B. F., & Pevunova, O. 2003, ApJS, 147, 29

TABLE 1
XMPG CANDIDATES

ID	g' (mag)	cz (km s^{-1})	Comment
SDSS J100539.35+315441.6	18.70	...	quasar?
SDSS J120955.68+142155.7	20.17	23340	metal poor galaxy
SDSS J123944.58+145612.8	19.77	21534	metal poor galaxy
SDSS J124638.82+350115.1	20.36	19522	metal poor galaxy
SDSS J124709.24+325118.6	19.10	27450	galaxy
SDSS J133424.53+592057.0	20.55	21890	metal poor galaxy
SDSS J135641.64+654748.8	19.72	10742	galaxy
SDSS J140439.28+542136.9	19.98	318	HII region
SDSS J141333.54+463234.0	19.43	90	A-star
SDSS J142250.72+514516.5	20.22	11654	metal poor galaxy
SDSS J143345.99-025602.2	19.69	65	A-star
SDSS J144158.32+291434.2	20.13	13741	metal poor galaxy
SDSS J145621.69+503523.0	20.49	...	BL Lac?
SDSS J150316.52+111056.9	19.41	23405	metal poor galaxy
SDSS J150535.89+314639.4	20.55	15817	galaxy
SDSS J151221.08+054911.2	20.15	24025	metal poor galaxy
SDSS J152802.62+240425.6	18.65	-6	A-star
SDSS J154742.23-005554.2	20.57	16594	E+A galaxy
SDSS J160238.71+444923.8	19.65	12350	galaxy
SDSS J165835.08+192415.3	18.93	-23	A-star
SDSS J172955.61+534338.8	19.55	24308	metal poor galaxy
SDSS J211613.97-000851.3	20.39	11916	galaxy
SDSS J221912.56+140602.8	20.41	36	A-star
SDSS J225900.86+141343.5	19.09	8918	metal poor galaxy

Izotov, Y. I., Papaderos, P., Guseva, N. G., Fricke, K. J., & Thuan, T. X. 2006a, A&A, 454, 137
Izotov, Y. I., Stasińska, G., Guseva, N. G., & Thuan, T. X. 2004, A&A, 415, 87
Izotov, Y. I., Stasińska, G., Meynet, G., Guseva, N. G., & Thuan, T. X. 2006b, A&A, 448, 955
Izotov, Y. I. & Thuan, T. X. 2004, ApJ, 616, 768
—. 2007, preprint astro-ph/0704.3842, 704
Izotov, Y. I., Thuan, T. X., & Guseva, N. G. 2005, ApJ, 632, 210
Kewley, L. J., Brown, W. R., Geller, M. J., Kenyon, S. J., & Kurtz, M. J. 2007, AJ, 133, 882
Kniazev, A. Y., Grebel, E. K., Hao, L., Strauss, M. A., Brinkmann, J., & Fukugita, M. 2003, ApJ, 593, L73
Kong, X. & Cheng, F. Z. 2002, A&A, 389, 845
Kunth, D. & Östlin, G. 2000, A&A Rev., 10, 1
Kunth, D. & Sargent, W. L. W. 1983, ApJ, 273, 81
Kunth, D., Sargent, W. L. W., & Kowal, C. 1981, A&AS, 44, 229
Kurtz, M. J. & Mink, D. J. 1998, PASP, 110, 934
MacAlpine, G. M., Smith, S. B., & Lewis, D. W. 1977, ApJS, 34, 95
Margutti, R. et al. 2007, A&A, preprint astroph/0709.0198
Masegosa, J., Moles, M., & Campos-Aguilar, A. 1994, ApJ, 420, 576
Massey, P., Strobel, K., Barnes, J. V., & Anderson, E. 1988, ApJ, 328, 315
McGaugh, S. S. 1991, ApJ, 380, 140
Osterbrock, D. E. 1989, Astrophysics of gaseous nebulae and active galactic nuclei (Mill Valley, CA: University Science Books)
Papaderos, P., Guseva, N. G., Izotov, Y. I., Noeske, K. G., Thuan, T. X., & Fricke, K. J. 2006, A&A, 457, 45
Prochaska, J. X. 2006, ApJ, 650, 272
Prochaska, J. X. et al. 2004, ApJ, 611, 200
Rego, M., Cordero-Gracia, M., Gallego, J., & Zamorano, J. 1998, A&A, 330, 435
Richer, M. G. & McCall, M. L. 1995, ApJ, 445, 642
Schaerer, D. & Vacca, W. D. 1998, ApJ, 497, 618
Schaller, G., Schaerer, D., Meynet, G., & Maeder, A. 1992, A&AS, 96, 269
Schlegel, D. J., Finkbeiner, D. P., & Davis, M. 1998, ApJ, 500, 525
Searle, L. & Sargent, W. L. W. 1972, ApJ, 173, 25
Shi, F., Kong, X., Li, C., & Cheng, F. Z. 2005, A&A, 437, 849
Sollerman, J., Östlin, G., Fynbo, J. P. U., Hjorth, J., Fruchter, A., & Pedersen, K. 2005, New Astronomy, 11, 103
Stanek, K. Z. et al. 2006, Acta Astronomica, 56, 333
Stasińska, G. 2005, A&A, 434, 507
Stasinska, G. 1980, A&A, 84, 320
Sutherland, R. S. & Dopita, M. A. 1993, ApJS, 88, 253
Terlevich, R., Melnick, J., Masegosa, J., Moles, M., & Copetti, M. V. F. 1991, A&AS, 91, 285
Tremonti, C. A. et al. 2004, ApJ, 613, 898
Vacca, W. D. 1994, ApJ, 421, 140
Wiersema, K. et al. 2007, A&A, 464, 529
Wolf, C. & Podsiadlowski, P. 2007, MNRAS, 375, 1049

TABLE 2
OBSERVED LINE INTENSITIES

F(λ_0 Ion)[a]	J120955.67 +142155.9	J123944.58 +145612.8	J124638.82 +350115.1	J133424.53 +592057.0	J142250.72 +514516.5	J144158.32 +291434.2	J150316.52 +111056.9	J151221.08 +054911.2	J172955.61 +534338.8	J225 +14
3727 [OII]	8.20 ± 0.22	11.8 ± 0.2	16.4 ± 0.4	22.5 ± 0.3	7.80 ± 0.14	5.70 ± 0.13	43.8 ± 0.5	9.00 ± 0.12	29.9 ± 0.5	15
3798 H10	···	0.84 ± 0.10	0.49 ± 0.06	0.62 ± 0.07	0.35 ± 0.07	0.27 ± 0.05	0.72 ± 0.09	0.36 ± 0.10	1.25 ± 0.11	1.2
3835 H9	···	0.29 ± 0.08	0.34 ± 0.06	0.55 ± 0.07	0.91 ± 0.10	0.45 ± 0.07	1.35 ± 0.12	0.35 ± 0.06	1.38 ± 0.11	1.3
3868 [NeIII]	1.75 ± 0.20	3.38 ± 0.14	4.09 ± 0.13	5.62 ± 0.11	6.11 ± 0.27	1.47 ± 0.12	14.5 ± 0.3	2.98 ± 0.23	13.5 ± 0.4	7.0
3889 He I + H8	0.66 ± 0.08	2.12 ± 0.17	1.86 ± 0.21	2.22 ± 0.11	3.14 ± 0.11	0.84 ± 0.10	5.43 ± 0.11	1.44 ± 0.11	5.09 ± 0.29	5.5
3968 [NeIII] + H7	1.07 ± 0.11	2.50 ± 0.11	2.39 ± 0.12	3.84 ± 0.14	4.78 ± 0.28	0.89 ± 0.09	8.67 ± 0.15	1.90 ± 0.11	8.21 ± 0.11	6.8
4101 Hδ	1.40 ± 0.11	2.50 ± 0.12	2.40 ± 0.23	3.60 ± 0.18	3.80 ± 0.11	0.90 ± 0.11	8.50 ± 0.19	2.30 ± 0.13	6.90 ± 0.14	7.9
4340 Hγ	2.70 ± 0.10	4.30 ± 0.11	4.40 ± 0.10	6.10 ± 0.10	8.30 ± 0.11	1.90 ± 0.11	15.9 ± 0.3	4.00 ± 0.11	12.4 ± 0.2	15
4363 [OIII]	0.30 ± 0.04	1.10 ± 0.13	1.00 ± 0.11	1.10 ± 0.10	2.00 ± 0.20	0.40 ± 0.07	3.50 ± 0.14	0.70 ± 0.09	2.90 ± 0.19	2.9
4471 He I	···	···	0.36 ± 0.06	0.32 ± 0.04	0.73 ± 0.09	0.29 ± 0.04	1.31 ± 0.11	···	···	0.6
4686 He II	···	···	0.19 ± 0.05	0.23 ± 0.04	0.73 ± 0.09	···	···	0.37 ± 0.05	0.41 ± 0.09	0.6
4861 Hβ	5.50 ± 0.11	10.4 ± 0.1	10.3 ± 0.1	14.1 ± 0.1	18.3 ± 0.2	4.00 ± 0.10	37.9 ± 0.4	9.80 ± 0.15	29.2 ± 0.4	33
4959 [OIII]	5.50 ± 0.24	15.1 ± 0.4	14.7 ± 0.1	20.8 ± 0.2	21.8 ± 0.2	4.50 ± 0.21	62.8 ± 0.6	11.9 ± 0.2	62.5 ± 0.7	33
5007 [OIII]	16.3 ± 0.2	45.0 ± 0.5	44.6 ± 0.5	61.8 ± 0.7	65.5 ± 0.7	13.6 ± 0.2	190.0 ± 1.9	35.2 ± 0.4	188.0 ± 2.2	100
5876 He I	0.46 ± 0.06	2.60 ± 0.11	1.18 ± 0.11	1.73 ± 0.12	2.08 ± 0.32	0.37 ± 0.05	3.73 ± 0.12	1.03 ± 0.11	3.76 ± 0.13	2.8
6563 Hα	14.8 ± 0.2	30.7 ± 0.4	31.5 ± 0.3	40.3 ± 0.7	46.2 ± 0.5	11.3 ± 0.1	102.0 ± 1.2	25.8 ± 0.3	94.2 ± 1.0	91
6584 [NII]	···	···	0.70 ± 0.08	1.30 ± 0.21	···	0.20 ± 0.03	1.90 ± 0.11	0.40 ± 0.05	1.40 ± 0.11	0.4
6678 He I	···	···	···	0.39 ± 0.06	···	···	0.94 ± 0.25	···	0.83 ± 0.09	0.4
6717 [SII]	1.40 ± 0.26	1.00 ± 0.16	1.40 ± 0.11	2.20 ± 0.11	0.70 ± 0.08	0.50 ± 0.09	3.70 ± 0.12	0.90 ± 0.10	3.20 ± 0.14	1.4
6731 [SII]	0.50 ± 0.08	1.00 ± 0.15	0.90 ± 0.13	1.30 ± 0.12	0.50 ± 0.09	0.30 ± 0.06	3.20 ± 0.11	···	2.20 ± 0.12	1.0
EW(Hβ)	54.4 ± 3.0	91.2 ± 5.0	70.7 ± 3.9	72.5 ± 4.0	95.9 ± 5.3	76.7 ± 4.2	80 ± 4.4	61.6 ± 3.4	158 ± 8.7	13

[a]Flux in units of $\times 10^{-16}$ ergs s^{-1} cm^{-2}. Uncertainties are statistical errors only, and do not include the errors due to reddening, stellar absorption, and abso calibration.

TABLE 3
OUR METAL POOR GALAXIES

ID	cz (km s^{-1})	M_B (mag)	T$_e$ (K)	log(O/H) + 12	Age (Myr)	Hα/Hβ	L(Hβ) (erg s^{-1})	SFR (T$_e$) (M$_\odot$ yr^{-1})	N(OB)	SN rate (10^{-4} yr^{-1})
SDSS J225900.86+141343.51	8918	-16.4	18600	7.37	4.0	2.75	1.80×10^{40}	0.21	13900	4
SDSS J142250.72+514516.49	11654	-15.9	19100	7.41	4.0	2.52	8.46×10^{39}	0.09	6500	2
SDSS J144158.32+291434.22	13741	-16.3	19400	7.47	4.5	2.80	1.08×10^{40}	0.13	10400	3
SDSS J080840.85+172856.48[a]	13233	-17.1	19000	7.48	4.5	2.64	1.94×10^{40}	0.18	18700	6
SDSS J123944.58+145612.80	21534	-17.7	17000	7.65	4.5	2.95	3.69×10^{40}	0.54	37400	12
SDSS J151221.08+054911.21	24025	-17.6	15300	7.68	5.5	2.64	2.63×10^{40}	0.32	40600	14
SDSS J120955.67+142155.91	23340	-17.4	15000	7.71	5.5	2.72	2.26×10^{40}	0.29	34900	12
SDSS J124638.82+350115.11	19522	-16.8	16200	7.75	5.0	3.06	1.61×10^{40}	0.26	24900	8
SDSS J150316.52+111056.93	23405	-18.3	14800	7.85	4.5	2.69	6.31×10^{40}	0.80	65800	22
SDSS J133424.53+592057.04	21890	-16.8	14500	7.86	5.0	2.86	1.73×10^{40}	0.23	27800	9
SDSS J172955.61+534338.80	24308	-18.3	13900	8.00	4.0	3.23	9.46×10^{40}	1.98	60800	20

[a]Kewley et al. (2007)